Pergamon

Stable isotopes in deep-sea corals and a new mechanism for "vital effects"

J. F. ADKINS,[1,]* E. A. BOYLE,[2] W. B. CURRY,[3] and A. LUTRINGER[1,4]

[1]Geological and Planetary Sciences, MS 100-23, Caltech, 1200 E California Boulevard, Pasadena, CA 91125, USA
[2]Earth, Atmosphere and Planetary Sciences, MIT, E34-200, Cambridge, MA 02139, USA
[3]Department of Geology and Geophysics, WHOI, Woods Hole, MA 02543, USA
[4]Laboratoire des Sciences du Climat et de l'Environnement, CNRS, Bat 12, av. de la Terrasse, FR-91198 Gif sur Yvette Cedex, France

Abstract—Offsets from isotopic equilibrium in biogenic carbonates have complicated paleoclimate reconstructions for decades. A new archive of climate, deep-sea corals, is used to evaluate the calcification processes, independent of photosynthesis, that contribute to these offsets. Carbon and oxygen stable isotope data from six modern deep-sea corals show strong linear trends between $\delta^{13}C$ and $\delta^{18}O$. Slopes of these trends between samples are similar and range between 1.9 to 2.6 for $\Delta\delta^{13}C/\Delta\delta^{18}O$. Linear trends intersect isotopic equilibrium for $\delta^{18}O$ and are slightly depleted for $\delta^{13}C$. Variations in the isotopic ratios are strongly correlated with the density banding structure. Isotopically depleted aragonite is associated with light, quickly precipitating bands, whereas isotopically enriched points correspond to slowly accumulating, less dense aragonite. The densest white band at the trabecular center is furthest from isotopic equilibrium for both carbon and oxygen. Data from this region fall off the linear trend between $\delta^{18}O$ and $\delta^{13}C$. This deviation, where $\delta^{13}C$ remains constant while the $\delta^{18}O$ continues to decrease, does not support "vital effect" mechanisms that call upon kinetic fractionation to explain offsets from isotopic equilibrium. We propose a new mechanism for vital effects in these deep-sea corals that is based on a thermodynamic response to a biologically induced pH gradient in the calcifying region. *Copyright © 2003 Elsevier Science Ltd*

1. INTRODUCTION

Oxygen isotopic variations in biogenic carbonates are a powerful tool for understanding the temperature of past climates. Urey (1947) established the theoretical basis for the $\delta^{18}O$ thermometer by calculating the relevant fractionation factors. McCrea (1950) verified these calculations with laboratory experiments of inorganic calcites. Epstein (1953) et al. measured mollusks from a variety of temperatures and demonstrated that this biogenic $CaCO_3$ is at isotopic equilibrium for $\delta^{18}O$. These studies established the basis for evaluating isotopic equilibrium in biogenic carbonates. Later work used the isotopic variations found in planktonic foraminifera to establish that the Pleistocene has been punctuated by large oceanic temperature shifts associated with glacial/interglacial cycles (Emiliani, 1966). These results were modified when it was recognized that fluctuations in global ice volume could account for more than half of the observed $\delta^{18}O$ signal (Shackleton, 1967; Dansgaard and Tauber, 1969). However, the global nature of marine $\delta^{18}O$ variations on glacial to interglacial time scales, and the recognition that they are paced by variations in the Earth's orbit, have led to the establishment of $\delta^{18}O$ as a key chronometer in paleoceanography (Hays et al., 1976). Decades of research have borne out Urey's original insight that the $\delta^{18}O$ of biogenic carbonates are a fundamental tool for reconstructing past climates.

Other impressive climatic information has come from stable isotopic studies of the skeletons of reef building surface-water corals. Because of the seasonal cycle's effect on the $\delta^{18}O$ of coralline aragonite, early work confirmed that the alternating light and dark density bands of coral skeletons represented annual accumulation (Fairbanks and Dodge, 1979). This result had been previously established by radiometric techniques (Knutson et al., 1972). In addition, long records from modern corals in the tropics record variations in the amplitude and period of the El Niño Southern Oscillation (ENSO; e.g., Cole et al., 1993). Holocene records have the potential to record how the ENSO signal is altered under different radiative forcing (McCulloch et al., 1996).

However, many of these paleoclimate studies are based on $\delta^{18}O$ signals that are out of isotopic equilibrium with respect to inorganic precipitates. Early work on benthic foraminifera demonstrated that different species growing in the same environment were offset in their $\delta^{18}O$ values, indicating that at least some species were offset from equilibrium (Duplessy et al., 1970). By sampling at high spatial resolution, McConnaughey (1989a) demonstrated that equilibrium offsets in coralline aragonite have a distinct spatial structure. Most climate studies, in both foraminifera and corals, circumvent this problem by assuming a time independent, constant offset from equilibrium and then interpret relative changes only. This offset is referred to as a "vital effect" (Weber and Woodhead, 1972). Understanding the chemical mechanism behind this effect has been a long-standing problem and a number studies have addressed key parts of it. For instance, isotopic measurements in foraminifera from controlled culture experiments show that the offset is correlated with the carbonate ion content of the growth environment (Spero et al., 1997). However, without considering the carbonate ion effect, evidence from sclerosponges shows that these animals precipitate at equilibrium (Böhm et al., 2000). For $\delta^{18}O$ in aragonite, it is difficult to establish true inorganic equilibrium because there are no controlled inorganic

---

* Author to whom correspondence should be addressed
(jess@gps.caltech.edu).

precipitation experiments. Why vital effects occur in some species and not others is an important question that limits geochemical studies of past climates. This article uses a new archive, deep-sea corals, to address that basic question.

McConnaughey (1989a) used the difference between symbiont bearing and nonsymbiont bearing coral species from the same growth environment to constrain the chemical mechanisms behind vital effects. His work established that the algal uptake of dissolved inorganic carbon (DIC) affects skeletal $\delta^{13}C$, presumably by leaving the residual inorganic calcification "pool" enriched in ^{13}C. He also documented a strong linear trend in $\delta^{18}O$ vs. $\delta^{13}C$ of the azooxanthellar coral *Tubastrea*, and ascribed this trend to a kinetic fractionation factor associated with the hydration of $CO_{2(aq)}$. Because this is the slow step in inorganic carbon speciation, McConnaughey calculated that it was possible for the coral to calcify faster than the hydration step could obtain isotopic equilibrium, thus preserving the kinetic fractionation in the skeleton. This kinetic fractionation mechanism is the widely accepted explanation for isotopic vital effects (McConnaughey, 1989b).

Several other studies have examined the calcification mechanism by using isotopic labeling techniques with corals either grown in culture or *in situ*. Symbiont containing corals from the Gulf of Eilat (*Stylophora pistillata*) show an $\sim11\times$ increase in calcification rate during the daytime (Erez, 1978). This increase also shows a trend to lighter $\delta^{18}O$ with increased photosynthesis (and generally higher calcification rates), in good agreement with McConnaughey's model. However, the $\delta^{13}C$ values showed depletion with higher photosynthetic rates. This contradiction may be rationalized as originating from "kinetically light" carbon overwhelming the photosynthetic enrichment, at least for this species at this location. Erez also documented a 5 to $10\times$ larger calcification rate when ^{45}Ca uptake was used as compared with ^{14}C uptake. This result implies that there is a carbon "pool" in the calcifying region that buffers skeletal carbon from the addition of tracer to the exterior environment. Detailed studies of the symbiotic coral, *Stylophora pistillata*, confirm the presence of a carbon pool and show that much of the skeleton in this species is derived from metabolic carbon as opposed to seawater DIC (Furla et al., 2000).

In this article, we use six modern deep-sea corals to further investigate stable isotopic vital effects. Because these species are free from the complications of photosynthetic symbionts and they grow in well characterized, homogeneous environments, deep-sea corals are an excellent taxonomic group for studying the effect of calcification alone on stable isotopic fractionation. Our linear trends between $\delta^{18}O$ and $\delta^{13}C$ agree with the more diverse sample set described in previous work (Smith et al., 2000). However, we use microsampling techniques to uncover a break in the $\delta^{18}O$ vs. $\delta^{13}C$ slope at the lightest values. Data from this newly formed aragonite show very light $\delta^{18}O$ values that do not fall on the linear trend formed by the rest of the skeleton. These data imply that a kinetic fractionation is not tenable as an explanation for our anomalous vital effects. This anomalous data motivated us to develop an alternative model for coral isotope fractionation that is based on thermodynamic responses to the enzyme-mediated chemistry of the semi-isolated calcification "pool."

Table 1. Equilibrium calculations for stable isotopes.

Variable	Sample			
	47407	78459	84820	A260-49
Temperature (°C)	5.5 ± 1.0	3.2 ± 0.3	5.6 ± 0.2	3.6 ± 0.2
Salinity[a]	34.2 ± 0.1	34.96 ± 0.02	34.56 ± 0.02	34.97 ± 0.02
$[PO_4]^{a}$ (μM)	1.8 ± 0.0	1.2 ± 0.1	2.8 ± 0.2	1.2 ± 0.1
$\delta^{18}O_{water}^{b}$ (‰)	0.3 ± 0.2	$0.3 \pm .1$	0.1 ± 0.1	0.3 ± 0.1
$\delta^{13}C_{DIC}^{c}$ (‰)	0.6 ± 0.4	1.0 ± 0.25	-0.2 ± 0.1	1.0 ± 0.25
$\delta^{18}O_{aragonite}^{d}$ (‰)	3.7 ± 0.7	4.5 ± 0.4	3.9 ± 0.2	4.4 ± 0.2
$\delta^{13}C_{aragonite}^{e}$ (‰)	3.3 ± 0.6	3.7 ± 0.5	2.5 ± 0.5	3.7 ± 0.5

[a] Estimated from Joe Reid Database (personal communication).
[b] Interpolated from data in Broecker (1986).
[c] Calculated from $[PO_4]$ regression and $\delta^{13}C$ of core tops in Duplessy et al. (1984).
[d] From Grossman and Ku (1986), Eqn. 1.
[e] From Romanek et al. (1992).

2. METHODS

Two types of images are used in this study. Transmitted light photonegatives are collected by polishing a ~200-μm-thick slab of coral that is epoxied to a glass slide. This "top view" is placed in a photographic enlarger and exposed as if it were a regular negative. Petrographic microscope images are made from true thin sections (~30 μm thick). Under cross-polarized transmitted light, a digital image is collected with a Nikon Cool Pix 990 camera and converted to gray scale in Adobe Photoshop software.

Samples for isotopic analysis are obtained by two different techniques. Breaking pieces by hand from either the septal or the thecal region of a single septum preserves little spatial information but provides large samples relatively quickly. Microsampling following a digitized image provides small amounts of carbonate at high spatial resolution with precise control of the sample's location. To obtain this spatial resolution, we use a computer-controlled micromill maintained at the Woods Hole Oceanographic Institution (Weidman et al., 1994). A coral slab is prepared by embedding the sample in epoxy on a glass slide and grinding it to the correct thickness (~200 μm) on a lap wheel. This is the same slab that is used to make the photonegative described above. The image is used to drive the micromill perpendicular to the banding pattern. Starting at the edge of the sample, the mill shaves successive layers from within the same band until there is ~40 μg of aragonite (~100 μm along the x-axis). The sample is collected, weighed, and placed directly into a Kiel device autosampler tube (see below). The remaining powder is removed by compressed air to ensure there is no cross contamination.

All isotopic data are collected on a Finnigan MAT-252 light gas mass spectrometer at the Woods Hole Oceanographic Institution. This machine is fitted with an automatic carbonate sample introduction system, the Kiel device, which uses a preset reaction time of 10 min. Two separate reaction lines are run simultaneously to save time during sample handling. All data are reported as per mil values and are corrected to the VPDB scale by comparison with the NBS-19 carbonate standard (Craig, 1957; Gonfiantini et al., 1995). A full description of the data correction procedures has been reported earlier (Ostermann and Curry, 2000).

Equilibrium values for the $\delta^{18}O$ and $\delta^{13}C$ of aragonite are estimated from the equations of Grossman and Ku (1986) and Romanek et al. (1992), respectively (Table 1). The equilibrium carbon isotopic values calculated by Romanek et al. use the $CO_{2(g)}$-HCO_3 fractionation factor determined by Mook et al. (1974). This value has recently been updated by Zhang et al. (1995) and has the potential to change equilibrium calculations for $\delta^{13}C$ by several tenths of a permil. Temperature, salinity and $[PO_4]$ are estimated from proximal hydrographic stations in the Joe Reid database (J. Reid, SIO, personal communication). Phosphate data were checked against nearby GEOSECS stations and are used to estimate the carbon isotopic ratio of the DIC in which the corals grew. We used the DIC $\delta^{13}C$ data in Duplessy et al. (1984) and our estimated phosphate concentration to generate the line, $\delta^{13}C_{DIC} =$

Trabecular Center
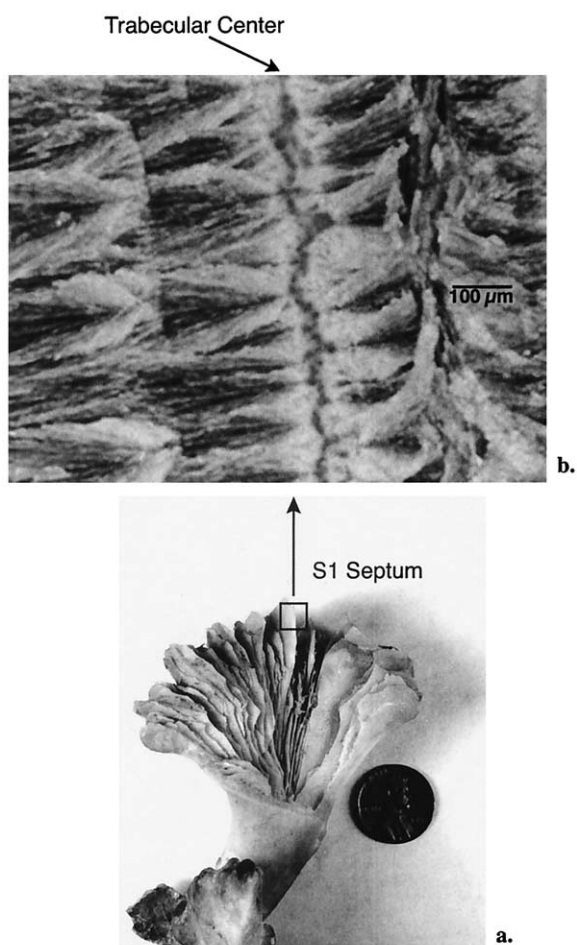

100 µm

b.

S1 Septum

a.

Fig. 1. Photographs of *D. cristagalli*. (a) Sample 36544 with half of the skeleton cut away to show where the single polyp sits within the radially symmetric septa. (b) Cross-polarized petrographic microscope image (5×) of the calcifying center (trabecula) from a single S1 septum. Small circles represent the nucleation sites for skeletal formation. Moving away from this trabecular plane, massive fine-grained crystals are followed by "bouquets" of aragonite needles. Light and dark needle packages correspond to the behavior of optically aligned crystals under the cross-polarized light.

1.863 to 0.716 × [PO$_4$] (r^2 = 0.96 over a [PO$_4$] range of 1.0 to 2.8 µmol/kg). Seawater oxygen isotopic values were estimated from the GEOSECS database as described in Broecker (1986).

One conclusion of this work, that follows previous studies (McCrea, 1950; Usdowski et al., 1991; Zeebe, 1999), is that pH is an important component of ^{18}O equilibrium. Currently, most studies use the temperature and the water oxygen isotopic value to define equilibrium δ^{18}O. We follow that practice here. However, we recognize that some sort of reference pH needs to be established to compare inorganic studies with biogenic precipitates. Even more importantly, further work on the mutual dependence of δ^{18}O values on pH and temperature needs to be performed with inorganic precipitates.

3. RESULTS

3.1. Calcification Images

The skeletal structure of *Desmophyllum cristagalli* has been extensively described elsewhere (Sorauf and Jell, 1977; Lazier et al., 1999). In Figure 1, we show the major coral hard parts

that are important to this work. Septa are radially symmetric around the individual polyp. The largest of these septa, the S1 series, all contain axial, visible white bands, which form the trabecular center. Under 5× magnification and cross-polarized light, several of the characteristic features of this central calcifying region are clearly displayed. The white band is a region of irregular fine crystals. Small circles form a chain of calcification centers, from which "bouquets" of aragonite needles radiate. It is clear from the cross-polarized light image (Fig. 1) that these crystal bunches are optically oriented. The exact relationship between the dark, possibly organic circles and the aragonite bouquets is not yet understood. However, it is clear from this image that the trabecular center (massive amorphous fine crystals) and the bulk of the rest of the septum (needle bouquets) are part of the same calcification process. Needle bouquets can be traced to individual spheres at the trabecular center. Densely packed fine crystals in the trabecula indicate rapid crystallization, whereas the long, well-organized needle bouquets indicate relatively slow growth conditions.

3.2. Hand Sampling

Results from hand sampling four individual deep-sea corals are shown in Figure 2. The most striking aspect of these data is the strong linear relationship between δ^{13}C and δ^{18}O. A single septum from one individual can span ~5‰ in δ^{18}O and ~12‰ in δ^{13}C. For *D. cristagalli,* these trends intersect isotopic equilibrium (black squares in Fig. 2), a fact that has been noted by previous work on this species (Smith et al., 2000). We cannot accurately estimate an aragonite equilibrium value for sample 36544 because we do not know the hydrography of the fjord in which it grew. However, the offset in δ^{18}O between this sample and the others indicates that the fjord waters are either fresher or warmer than the open ocean. Slopes of δ^{18}O vs. δ^{13}C for all individuals in this article fall in the narrow range of 1.9 to 2.6 (Table 2). Standard errors on the slopes average about ±0.1 and demonstrate that small differences among the several samples are significant at the 95% confidence limit. Although the data from the one *Lophelia* sample falls at the low end of the *D. cristagalli* data, it still overlaps with two other samples. Overall, the slope differences between samples of different genera are not large, but they are distinguishable.

The most outstanding characteristic of the *Lophelia* sample is its large offset from equilibrium. By extrapolating the measured data to the δ^{18}O equilibrium value, it is clear that the δ^{13}C of AII-260-49 is depleted in ^{13}C by over 3‰. As will be discussed later, this effect is probably due to the incorporation of a significant amount of respired carbon into the *Lophelia* skeleton. This effect is not observed in the other samples. It is clear in the *D. cristagalli* corals that the septal aragonite is more homogenous than the thecal CaCO$_3$ and that thecal material tends to be more isotopically depleted than the septum. We investigated this trend further by microsampling two separate *D. cristagalli* samples.

3.3. Microsampling

Along with the coral's banding pattern, oxygen isotopic results from microsampling Pacific sample 47407 are shown in Figures 3 and 4. Banding patterns in these figures are from the
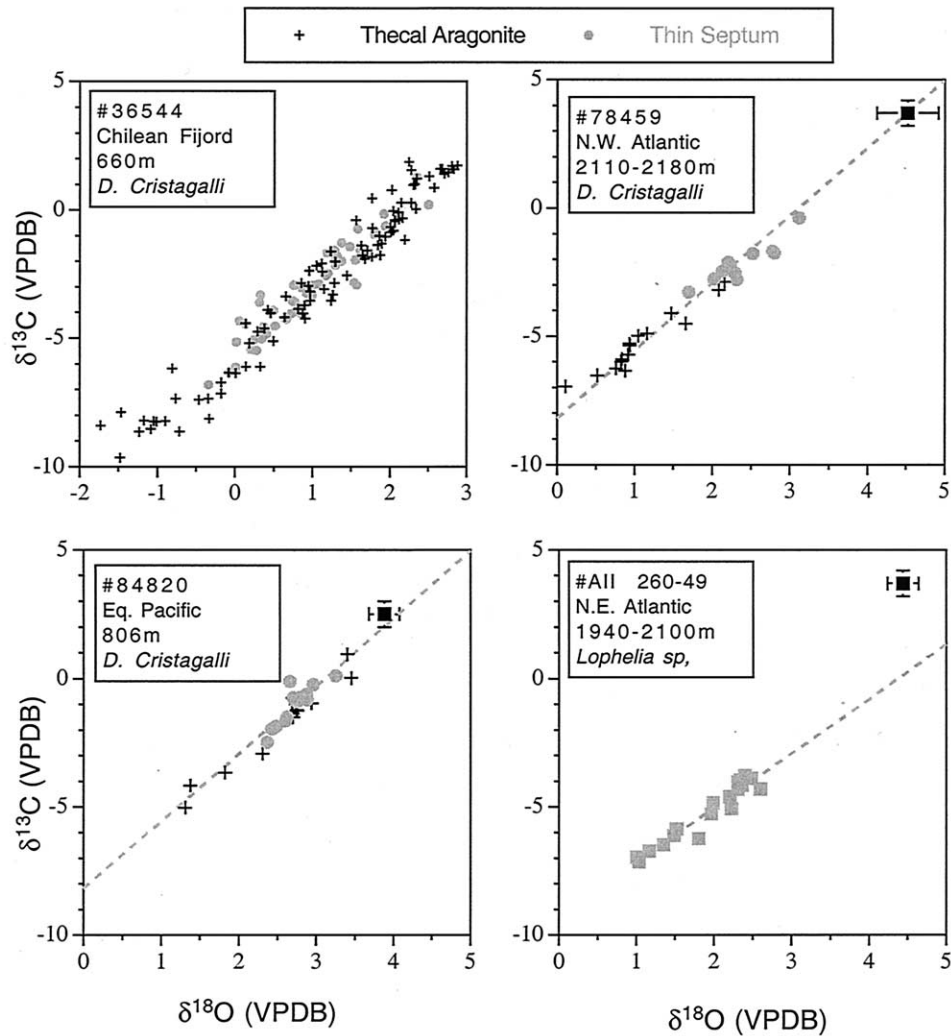
Fig. 2. Stable isotope data from single septa on four modern deep-sea corals. Black squares indicate the estimated aragonite equilibrium value for the open ocean sites where there is near by hydrographic data. Plus signs are from the thecal aragonite, the outer rim of the skeleton where septa join together. Gray circles are from the thin septum. Dashed lines are the best linear fit to the data. D. *cristagalli* trends clearly intersect isotopic equilibrium, whereas the *Lophelia* sample is several permil depleted in δ^{13}C relative to δ^{18}O.

photonegative images described in the Methods section. Microsampling milled a swath across the coral slab that is as wide as the y-axis in Figure 3 is long. Plateaus in δ^{18}O represent the distance required to microsample enough $CaCO_3$ to make a measurement. There is a clear association between the arago-nite's optical density and its isotopic value. White bands are always more depleted in δ^{18}O than dark bands. Because these are negative images, white bands are optically denser than their darker counterparts. Where two septa meet in the thecal region (Fig. 3) there is a "confused" banding pattern and the isotopic

Table 2. Regression statistics for deep-sea coral stable isotopes. For microsampled corals 36544, 47407, and JFA 41.12, the regression statistics are for the linear trends excluding points from the trabecular centers.

| Sample	Species	Depth (m)	Latitude	Longitude	Slope	2σ error	Intercept (‰)	2σ error	Fit r^2
78459	*D. cristagalli*	2110–2180	38.45°N	72.39°W	2.24	0.17	−7.53	0.29	0.97
84820	*D. cristagalli*	806	0.14°N	91.36°W	2.59	0.31	−8.74	0.89	0.91
All-260-49	*Lophelia*	1940–2100	33.36°N	62.26°W	2.16	0.32	−9.98	0.71	0.92
36544	*D. cristagalli*	636	51.52°S	73.41°W	2.59	0.11	−5.62	0.15	0.94
47407	*D. cristagalli*	549	54.49°S	129.48°W	2.36	0.13	−6.53	0.35	0.97
JFA 41.12	*D. cristagalli*	1000–2000	38°12.3'N	26°26.1'W	1.94	0.12	−6.55	0.12	0.99
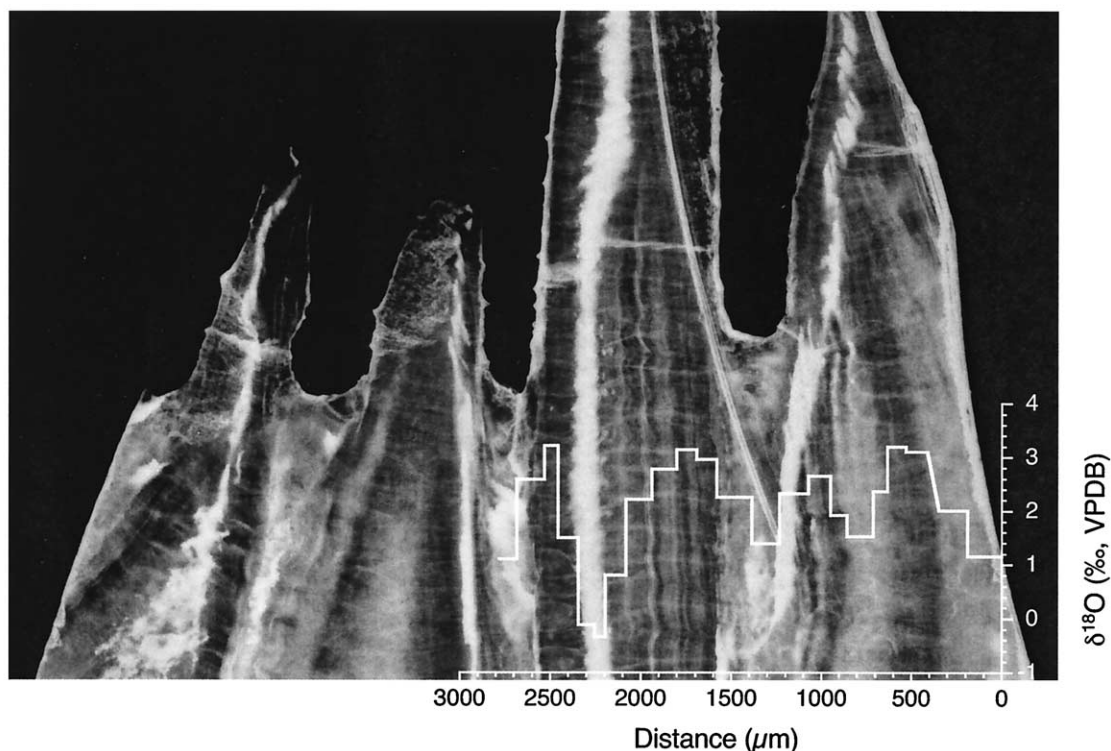
Fig. 3. $\delta^{18}O$ results from microsampling the thecal region of *D. cristagalli* sample 47407-G. Banding is due to the optical density variations in the ~200-μm-thick slab. The trabecular center of the large S1 septum is the white band at 2300 μm. The curved line near this band is a scratch on the glass slide. Banding in the other smaller septa is clearly different than the original S1 septum. Each isotopic point represents an ~150-μm-long swath with a microsampler that is as wide as the $\delta^{18}O$ axis. Approximately 40 μg of powder was collected for each measurement. There is a clear correlation between the banding pattern and the $\delta^{18}O$ value.

data lie between the dark and light extremes reflecting this complicated structure. Within the theca, bands in the smaller side septa are wider than those in the large S1 septum and still show the trend between isotopes and banding. In Figure 3, the largest spatial gradient in isotopic value is between the white trabecular center and the adjoining material of the S1 septum. Because $\delta^{13}C$ is tightly correlated to $\delta^{18}O$ in this region, the carbon isotope data show identical results and are not reproduced in a separate figure. Within the thin septal material (Fig. 4, sample 47407-2A), there is an even larger spatial gradient between the dark bands and the optically dense trabecular center. Over a distance of ~50 μm, there is a >5‰ drop in $\delta^{18}O$.

Figure 5a shows the same data from the previous two figures as a plot of $\delta^{18}O$ vs. $\delta^{13}C$. The dark bands on the thinnest portion of the septa are at isotopic equilibrium for $\delta^{18}O$. Although they also have the heaviest $\delta^{13}C$ values, the data are slightly depleted relative to aragonite equilibrium for this isotope. Microsampling data for two other deep-sea corals are also shown in Figures 5b,c. Because the spatial patterns of these isotopic data, relative to the banding, display the same trends as those shown in Figures 3 and 4, we do not reproduce them here. For the data in gray circles, trends of $\delta^{18}O$ vs. $\delta^{13}C$ for all three samples have the same slope as the other *D. cristagalli* samples we analyzed (Table 2). However, the black squares in Figure 5 show a deviation from this linear trend. All of these points are from the trabecular center on the thin portion of the S1 septa

(white band in Fig. 4). For sample 36544 (Fig. 5b), we collected two points from the same white band on a single transect. For sample JFA 41.12 (Fig. 5c) we collected many trabecular centers from several different septa on the same coral, and from several different transects on the same septum. Thus, in all of our microsampled data the trabecular band on the thinnest portion of the S1 septum shows a deviation from the otherwise ubiquitous linear trend in stable isotope values. This observation is the basis for our reinterpretation of the "kinetic" model for skeletal isotopic fractionation in corals.

4. DISCUSSION

An understanding of the chemistry in the calcifying region is essential to account for the mechanisms underlying the carbon and oxygen isotope fractionations. Because surface and deep corals are both scleractinians, we utilize the extensive literature about calcification in zooxanthellar corals to inform our discussion of the deep-sea samples (Goreau, 1959; Johnston, 1980; Furla et al., 2000). There are two key advantages to studying calcification in *D. cristagalli* in particular and deep-sea corals in general. First, the lack of algal symbionts eliminates photosynthesis as a source of isotopic variation. As mentioned above, McConnaughey (1989a) established that for a given $\delta^{18}O$ value in the skeleton azooxanthellar corals are depleted in $\delta^{13}C$ compared with corresponding photosynthetic species. He attributed this difference to the preferential uptake
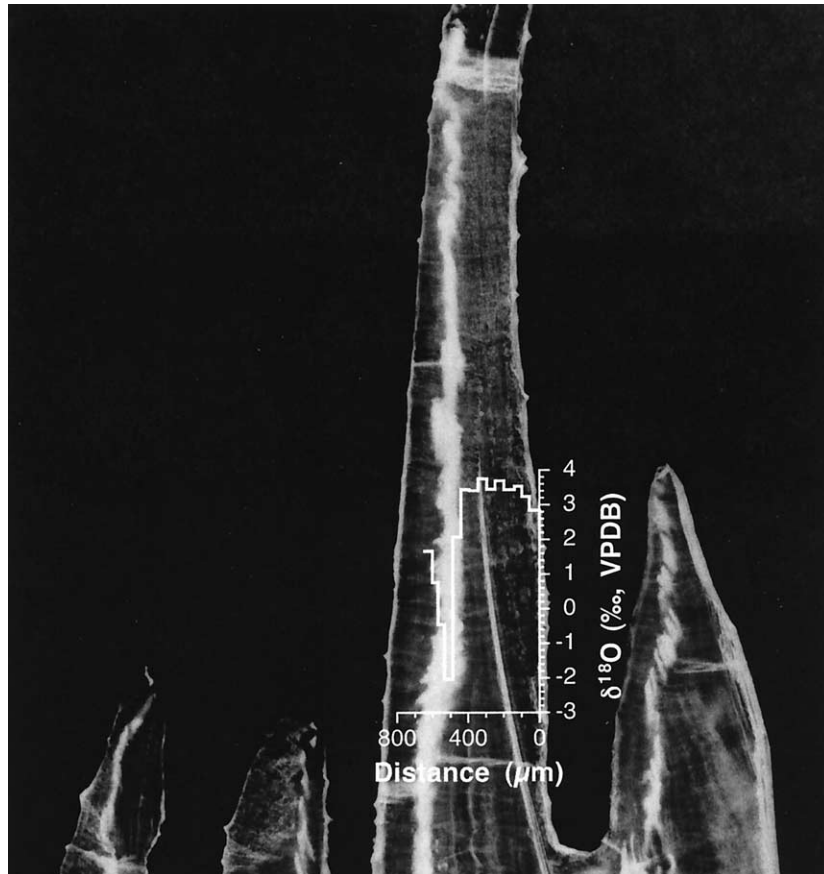
Fig. 4. Similar to Figure 3, but for the thin septal region of sample 47407-2A. The isotopically depleted band at 500 μm is from only the optically dense white band.

of ^{12}C over ^{13}C during carbon fixation by the symbionts living in the coral tissue. This aspect of McConnaughey's model has been used to correct raw $\delta^{13}C$ values for their "kinetic" contribution to better constrain the variations in photosynthesis and heterotrophy (Heikoop et al., 2000). Azooxanthellar species do not have this photosynthetic complication.

A second advantage is that corals from a deep marine environment grow in a constant temperature, constant salinity and constant isotopic composition of water that can be estimated relatively accurately. Without having to manipulate them in culture, the *D. cristagalli* samples are calcifying in a very controlled medium that allows us to calculate the expected isotopic equilibrium values for each sample. Here we present a possible explanation for why the data deviate from this inorganic equilibrium value.

The key observation is that $\delta^{13}C$ vs. $\delta^{18}O$ trends are linear until the lightest values where $\delta^{18}O$ continues to decrease but $\delta^{13}C$ does not change (Fig. 5). Figure 5c shows results from several microsampling transects from within the same coral. Though trabecular $\delta^{13}C$ data are not always the lightest values in the entire coral, for an individual transect the trabecular center (black squares) is always the most ^{13}C depleted and falls off the line. This feature cannot be explained by mixing of two end members with different isotopic compositions. This type of mixing can sometimes result in curves that approximate the data in Figure 5. However, it cannot account for the deviation

from a constant slope. In the case of solid carbonates, both the carbon and oxygen atoms are attached to the same molecule, thus demanding that the bulk concentrations of each element within an end member (the total dissolved carbon concentration, not the $\delta^{13}C$ and $\delta^{18}O$) are equal. Mixing curves in this case degenerate to straight lines.

In an effort to understand the cause behind the deviation from a line at the lightest trabecular oxygen isotope values, we now explore an alternative model for the relationship between $\delta^{13}C$ and $\delta^{18}O$ in corals. There are three important features to explain; a constant $\delta^{18}O$ vs. $\delta^{13}C$ slope, a deviation to nearly constant $\delta^{13}C$, for an individual microsampling transect, at the lightest $\delta^{18}O$ values, and the numerical value of the slope itself. We assume that all portions of the coral skeleton are precipitated by the same process and use a single model to explain the data. The system could be more complicated than this approach. We use the following model to demonstrate that the constant slope, and then a deviation from this slope at the lightest values, can be simply explained by thermodynamics of the system and the coral's enzymatic machinery. Further complications to this basic model might include kinetic effects when there is no carbonic anhydrase present, or complications from organic templates in the trabecular centers. The strong correlation between the inferred calcification rate (light and dark bands) and isotopic composition, as well as the crystal
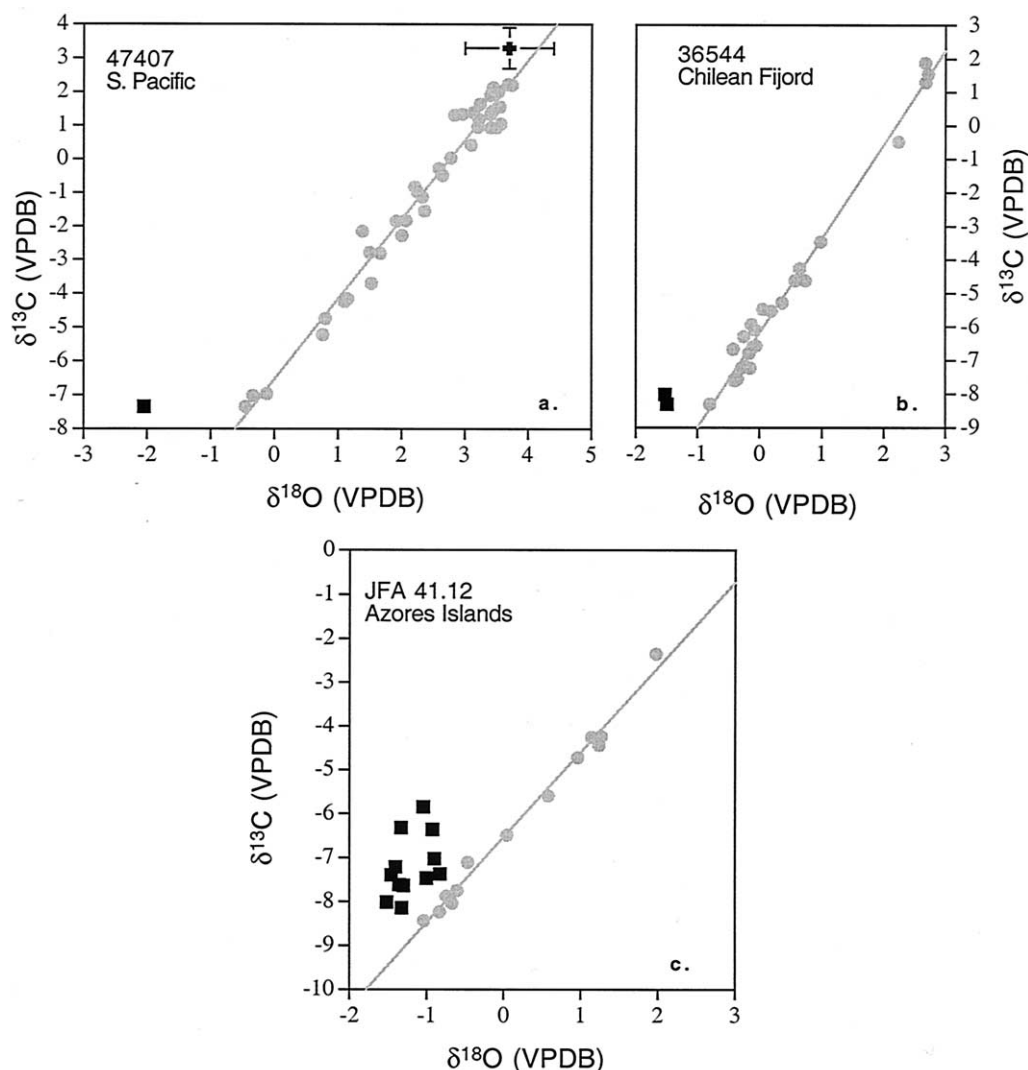
Fig. 5. Stable isotope results from microsampling three *D. cristagalli* samples. In all graphs, black squares are samples from the optically dense (white) bands of the trabecular centers. Gray circles are from all other parts of the skeleton. (a) Data from Figures 4 and 5 plotted vs. $\delta^{13}C$. The heaviest points from Figure 5 are at equilibrium (black cross) for $\delta^{18}O$ but are slightly depleted in $\delta^{13}C$. (b) Sample 36544 from a fjord in southern Chile, where there is no hydrographic information to estimate isotopic equilibrium. (c) Sample JFA 41.12 from the Azores Islands. These data represent many microsampling transects from separate septa and different locations on the same septum. All samples from the trabeculae show a deviation from the linear trend at the lightest isotopic values.

structure itself (Fig. 1), all imply that a single model is a reasonable beginning.

In the following sections, we will do the following: (4.1) examine the role of incorporated metabolic carbon in skeletons of deep-sea corals; (4.2) outline the relevant transport pathways and chemical reactions in the calcifying mother liquor (and also summarize McConnaughey's kinetic theory for fractionation); (4.3 and 4.4) propose a new explanation for vital effects that can explain many features of the biogenic data; and (4.5) develop a numerical model of our proposed new mechanism.

4.1. Metabolic Carbon

Because the organic matter consumed by organisms in the ocean is strongly depleted in ^{13}C relative to the inorganic

carbon pool, the presence of metabolically derived CO_2 in skeletal $CaCO_3$ will complicate any model of isotopic fractionation during calcification. Although oxygen seems to achieve isotopic equilibrium on the less dense, slowly calcifying portions of the thin S1 septa of *D. cristagalli* (Fig. 5), carbon isotopes are variably offset from calculated equilibrium. By extrapolating the linear trends in Figure 2 to $\delta^{18}O$ equilibrium, it is clear that in *D. cristagalli* the $\delta^{13}C$ offset is small, but in *Lophelia* sp., the carbon offset is over 3‰. Fortunately, radiocarbon can be a very powerful tracer of the amount of metabolically derived carbon that ends up in a coral's skeleton. As filter feeders, modern deep-sea corals are potentially consuming organic matter labeled with bomb radiocarbon. In contrast, they are calcifying in waters that are depleted in radiocarbon

relative to the atmosphere. This effect is especially strong in the intermediate waters of the tropical Pacific, where some of the oldest waters of the modern ocean are located, yet biologic production, the coral's food supply, has a bomb-contaminated ^{14}C signature.

We have measured the $\Delta^{14}C$ of 12 modern deep-sea corals from seven different genera (Adkins, 1998). Within measurement error, all of the data are consistent with ambient deep-water inorganic carbon as the only source of skeletal carbonate. However, we have analyzed one sample from Station M (34°50'N, 123°00'W) in the tropical Pacific that falls on a 1:1 line with ambient inorganic $\Delta^{14}C$ but has 2σ error bars that are as high as 10‰ above the ambient value. This *Fungiacyathus marenzelleri* (NMNH 93177) was collected from a depth of 4100 m and provides a constraint on the maximum amount of metabolic CO_2 that could be in the coralline aragonite. Druffel et al. (1996) analyzed the radiocarbon content of the suspended and sinking fraction of the dissolved organic carbon at Station M. With these data on the $\Delta^{14}C$ of the metabolic carbon end member, we can write a mass balance equation for the $\Delta^{14}C$ of the deep-sea coral skeleton:

$$\Delta^{14}C_{skeleton} = x\Delta^{14}C_{food} + (1-x)\Delta^{14}C_{seawater} \quad (1)$$

where x is the fraction of the skeleton that comes from metabolic carbon. Rearranging this equation to solve for the $\Delta^{14}C$ of the food gives

$$\Delta^{14}C_{food} = \frac{10}{x-230} \quad (2)$$

Here, −230‰ is the ambient $\Delta^{14}C$ of DIC from nearby GEO-SECS site 347 (Ostlund et al., 1987) and 10‰ is the maximum offset between coral and seawater $\Delta^{14}C$ allowed by the error bars on the data (Adkins, 1998). Figure 6 illustrates this hyperbola with the particulate organic carbon (POC) data from Druffel et al. (1996). Although 0% metabolic carbon in the skeleton is still a possible result, the maximum amount of nonambient DIC possible is ~8%. The exact amount is dependent on the POC food source and the errors on the coral $\Delta^{14}C$ measurement of the skeleton. A similar calculation for ^{13}C, using a particulate $\delta^{13}C$ of −20‰, implies a metabolic carbon contribution to skeletal $\delta^{13}C$ of about −1.0‰. This result is consistent with the *D. cristagalli* data in Figures 2 and 5. In these samples, the $\delta^{13}C$ extrapolated to $\delta^{18}O$ equilibrium is slightly depleted. Where we have clearly measured the $\delta^{18}O$ at equilibrium (Fig. 5), the $\delta^{13}C$ offset is ~0.6‰. Our one *Lophelia* sp. sample seems to have a much larger contribution of metabolic carbon in its skeleton. However, for both species it is impossible to explain the linearly correlated offsets from equilibrium with metabolic carbon alone. These results are in stark contrast to the data for surface, symbiont-bearing coral species (Pearse, 1970; Erez, 1978; Furla et al., 2000). However, this discrepancy is not surprising because the bulk of the evidence indicates that the metabolic carbon in coralline aragonite results from the direct transfer of carbon from the symbionts to the coral. This pathway is not available in azooxanthellar corals.
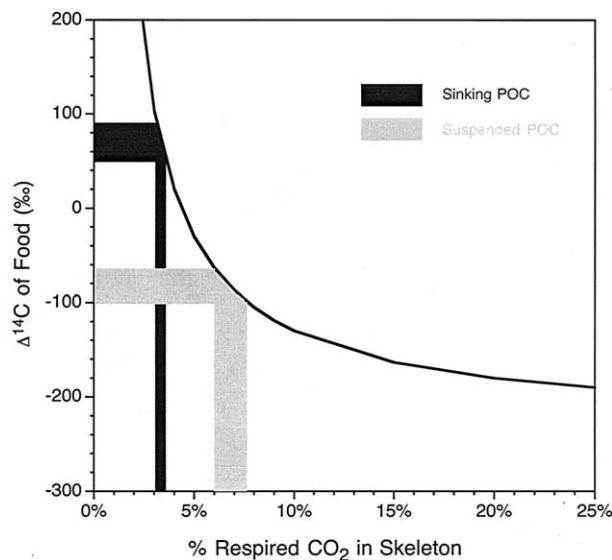

Fig. 6. Radiocarbon-based sensitivity calculation of the amount of skeletal carbon that can originate from metabolic CO_2 produced by the coral polyp. The black hyperbola represents all the possible combinations of respired CO_2 content and $\Delta^{14}C$ of the coral's food source that satisfy the $\Delta^{14}C$ data from the surrounding DIC and the measurement of the skeleton (see text). Radiocarbon contents of the sinking and suspended particulate fraction from this site are from Druffel et al. (1996). The particulate data constrain the maximum amount of respired CO_2 in the skeleton to be less than 8% of the total.

4.2. Extracellular Calcifying Fluid and McConnaughey's Kinetic Mechanism

The "mother liquor" from which coralline solids precipitate is located between the skeleton and the coral's calicoblastic membrane. All calcium carbonate formed by the coral must be deposited in association with this calicoblastic tissue and is therefore organically mediated. McConnaughey referred to this mother liquor region as the extracellular calcifying fluid (ECF). Figure 7 is a schematic of the area around the ECF that largely follows McConnaughey's representation, which itself was adapted from Johnston (1980). The cell membrane, a lipid bilayer, is impermeable to ionic transport. This means that Ca^{++} can be transported to the ECF by two pathways. Either it leaks in from the surrounding seawater, as in an open system, or it must be pumped by an enzymatic system, here represented by Ca-ATPase (Ip et al., 1991). By this mechanism, calcium is deposited and protons are removed from the ECF, thus making the enzyme a very effective alkalinity pump and maintaining a large pH gradient across the cell membrane (Furla et al., 2000). It is possible that a Mg/Ca exchanging enzyme system could also be used by scleractinia to pump Ca ions, but recent work with inorganic precipitation studies has shown that this process is less efficient at forming $CaCO_3$ solid than the direct alkalinity pump (Zeebe and Sanyal, 2002).

Transport of inorganic carbon to the ECF is more complicated than for calcium. Of the inorganic carbon species, only $CO_{2(aq)}$ is uncharged and can move freely across the cell membrane. For bicarbonate and carbonate ions, either another enzymatic system is required, or they leak into the ECF from
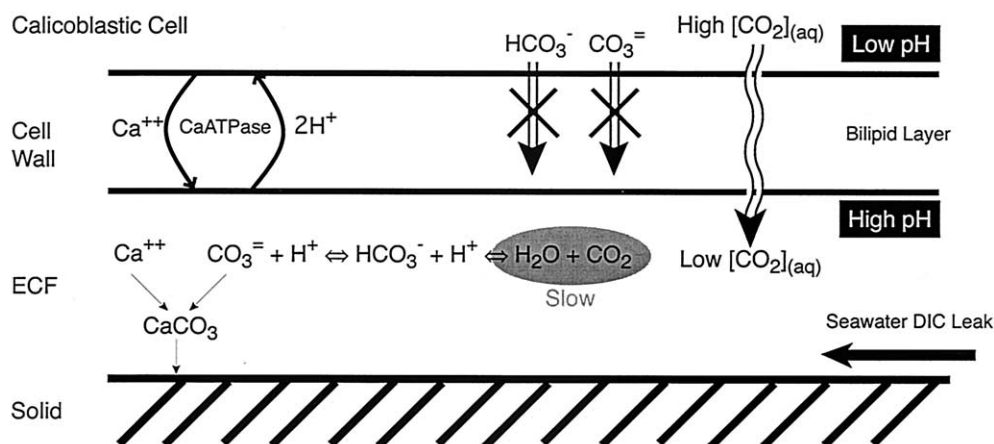
Fig. 7. Schematic of the coral calcifying region (McConnaughey, 1989a). The cell membrane is impervious to passive ionic transport. Calcium cations are enzymatically pumped into the skeletal mother liquor, or ECF, setting up a large pH gradient between the calcifying region and the cell/surrounding seawater. Carbon enters the ECF via diffusive transport of $CO_{2(aq)}$ across the cell membrane or via diffusion from the surrounding seawater. Hydration of $CO_{2(aq)}$ is the slow step in inorganic carbon speciation. Carbonic anhydrase, if present in the ECF, catalyzes this exchange. The ECF is ~10 μm wide.

seawater. For $CO_{2(aq)}$, either pathway, from across the calicoblastic membrane or from seawater leakage, will require the hydration of $CO_{2(aq)}$ to precipitate carbonate. McConnaughey located the cause of the linear trend in $\delta^{18}O$ and $\delta^{13}C$ at this inorganic speciation step (Fig. 7). The hydration of $CO_{2(aq)}$ is the slow step in inorganic carbon kinetics (Johnson, 1982). With a series of calculations, McConnaughey showed that a kinetic fractionation factor associated with the forward hydration reaction could be expressed in the skeleton. By this model, a kinetic fractionation could be preserved in the solid if precipitation rates are faster than the establishment of equilibrium in the $CO_{2(aq)} + H_2O$ system. Therefore, points along the $\delta^{13}C$ vs. $\delta^{18}O$ line (Figs. 2 and 5) are the result of more (lighter values) or less (heavier values) of the kinetic fractionation being expressed in the biogenic solid. The extent of kinetic fractionation is correlated with the calcification rate and, in the deep-sea corals, with the banding pattern. However, as long as all parts of the skeleton are formed by the same process, the enriched $\delta^{13}C$ values that fall off the linear trend in Figure 5 negate this kinetic hypothesis. Because the oxygen and carbon atoms are in the same molecule, there is no way for a kinetic fractionation factor to generate a change in slope between $\delta^{18}O$ and $\delta^{13}C$. In a kinetic model, carbon cannot stop fractionating while oxygen continues to discriminate against ^{18}O. In addition, carbonic anhydrase, an enzyme that catalyzes the conversion of bicarbonate to $CO_{2(aq)}$, has been identified in coral tissue (Ip et al., 1991). Although this evidence does not prove that the enzyme is in the ECF, it's presence ensures that the inorganic carbon system is at equilibrium. A new model of isotopic fractionation in biogenic carbonates is necessary as kinetic fractionation does not explain the deep-sea coral data. Microscopic observations suggest that $CaCO_3$ is formed in association with vacuoles pinched off from calicoblastic cells (Johnston, 1980). Although these spheres complicate the geometry shown in Figure 7, they do not change the basics of the biology and chemistry described below.

4.3. Alternative Model for Vital Effects: Carbon

Given that neither metabolic carbon nor kinetic effects can explain the anomalous data, we propose a new mechanism for vital effects in deep-sea corals and separate the discussion into carbon and oxygen effects. The two discussions are then combined into a single proposed mechanism. The $\delta^{13}C$ trend found in deep-sea corals is related to the impermeability of the ECF membrane to ionic transport. CO_2 is the only inorganic carbon species that can passively move across this barrier (Fig. 7). Because of the alkalinity pump of Ca-ATPase (and/or proton ATPase), there are large pCO_2 and pH gradients across this membrane that, at any particular time, are dependent on the enzyme's activity. This gradient drives passive diffusion of CO_2 into the ECF. When the pH of the ECF is high (high calcification rate, high Ca pumping), the inventory of carbon in the mother liquor pool is very small relative to the rate of skeletal formation. This relationship means that the outgoing carbon, the skeleton, must approach the isotopic value of the incoming carbon. This later value is a function of the relative rates of CO_2 entering the ECF from across the cell membrane and from seawater via open channels (a "leaky pool"). At thermodynamic equilibrium, the depletion of the $\delta^{13}C$ of CO_2 with respect to the $\delta^{13}C$ of aragonite is ~13‰ at 5°C (Romanek et al., 1992; Zhang et al., 1995). In a closed system ECF, fed only by membrane crossing CO_2, the skeleton would quickly take on this very light isotopic value. However, the system is not closed. Depending on the geometry of the ECF itself, seawater can more or less easily diffuse into the calcifying region (Fig. 7). The resulting mixture of ^{13}C-depleted, membrane crossing CO_2 and "normally" speciated inorganic carbon ($\delta^{13}C$~1.0‰) determines where in $\delta^{13}C$ space a coral sample lies on the linear trends in Figures 2 and 5. Fast calcification (white bands in Figs. 3 and 4) results from an active alkalinity pump, which leads to a large pCO_2 gradient and therefore a large component of "membrane" carbon relative to seawater carbon. Slow calcification (dark bands in Figs.

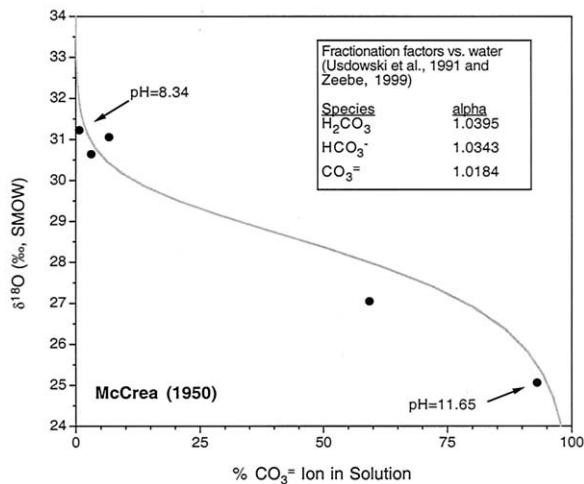Fig. 8. Illustration of pH's effect on the $\delta^{18}O$ of DIC. McCrea's (1950) early work demonstrated a relationship between the %CO_3 in solution and the $\delta^{18}O$ of the solid carbonate precipitated from that solution. Later, more thorough experiments by Usdowski et al. (1991) and Usdowski and Hoefs (1993) demonstrated that there were separate oxygen fractionation factors (alphas) between each of the inorganic carbon species and H_2O. This relationship results in an overall depletion of $\delta^{18}O$ in DIC at higher pHs. If this carbon is either quantitatively removed or precipitated such that the $HCO_3^-/CO_3^=$ ratio is preserved in the solid, carbonates formed from more acidic solutions will have heavier $\delta^{18}O$ values. This trend is consistent with the pH-driven depletions in $\delta^{13}C$ observed in deep-sea corals (see text).

3 and 4) allows the ECF to more thoroughly mix with ambient seawater and promotes heavy $\delta^{13}C$ in the skeleton. When skeletal $CaCO_3$ is constructed at the maximum flux of CO_2 from across the cell membrane, the $\delta^{13}C$ cannot become any lighter. This maximum occurs when the pH of the ECF rises to the point where CO_2 concentrations are very low. At this point the $\delta^{13}C$ of the skeleton obtains its furthest offset from equilibrium.

4.4. Alternative Model for Vital Effects: Oxygen

Although this mechanism explains the $\delta^{13}C$ range, we still need to understand the $\delta^{18}O$ trend, and the reason for the nearly constant $\delta^{13}C$ at light $\delta^{18}O$ values (for an individual micro-sampling transect). In this new model, oxygen isotopic fractionations are also the result of an enzymatically induced pH gradient, but for a very different reason than for carbon. The oxygen portion of the model is based on three previous studies. McCrea's seminal work on the temperature and pH effects of $\delta^{18}O$ fractionation in carbonates showed a dependence of the solid $\delta^{18}O$ on the %CO_3 ion in solution (McCrea, 1950). He precipitated $CaCO_3$ solids from solutions of the same temperature and water $\delta^{18}O$, but different pHs, by adding $CaCl_2$ far in excess of the $CaCO_3$ K_{sp}. Over his full range of %CO_3 in solution (from pH = 8.34 to 11.65), McCrea found a 6‰ range in the $\delta^{18}O$ of the inorganic carbonates, where more basic solutions corresponded to lighter $\delta^{18}O$ (Fig. 8). Usdowski demonstrated that McCrea's data are consistent with the fact that oxygen atoms in each of the separate inorganic carbon species have separate offsets from water $\delta^{18}O$ (Usdowski et al., 1991; Usdowski and Hoefs, 1993). By use of more careful

experiments in buffered systems, these authors showed that carbonate ion has the smallest fractionation factor (α = 1.0184), whereas carbonic acid has the largest offset from water (α = 1.0395). In all cases the oxygen in inorganic carbon species is more enriched in ^{18}O than it is in seawater, and solutions with higher [CO_3] are isotopically lighter than more acidic waters. In McCrea's experiments enough $CaCl_2$ was added to the carbonate solutions to precipitate all of the DIC in his beakers. In this case, the $\delta^{18}O$ of the solid formed is determined by the total number of ^{18}O and ^{16}O atoms attached to DIC species. Because this number is dependent on the proportions of carbonate ion, bicarbonate ion, and carbonic acid (the DIC speciation), the $\delta^{18}O$ of the solid must be dependent on the pH of the mother liquor.

For coraline aragonite, this pH dependence of $\delta^{18}O$ holds only if the calcium carbonate forms from a mixture of inorganic carbon species in proportion to their ratios in the ECF. Zeebe (1999) showed that this criterion is met for both the foraminifer *Orbulina universa* (Spero et al., 1997) and the synthetic carbonates of Kim and O'Neil (1997). Zeebe demonstrated that either all of the inorganic carbon in the ECF is quantitatively precipitated as $CaCO_3$ or the solid is made from both HCO_3^- and $CO_3^=$ in proportion to their ratio in the ECF (i.e., by vacuole formation). This is a fundamentally different type of isotopic fractionation than the carbon system. For carbon there are a finite number of ^{13}C atoms that are partitioned among the inorganic species. An organic membrane "selects" for the isotopically lightest of these species by being impervious to ionic transport. For oxygen, there is an "infinite" reservoir of ^{18}O atoms in the surrounding water. However, the individual DIC species have separate offsets from this water $\delta^{18}O$ value. The total number of ^{18}O atoms that end up in the inorganic carbon pool is dependent on the DIC speciation itself. More basic solutions will have fewer ^{18}O atoms, relative to ^{16}O, in the DIC than will lower pH solutions.

The fact that inorganic carbonates show the Usdowski et al. (1991) fractionation is puzzling. If the solid is being formed from carbonate ion, it should have a constant $\delta^{18}O$ that is ~18.4‰ offset from the water value, plus any effect due to the temperature of precipitation. However, Zeebe (1999) demonstrated that this is not the case for the three data points in the inorganic precipitation experiments of Kim and O'Neil (1997) where temperature (19°C) and water $\delta^{18}O$ were held constant but the initial pH was different. This result implies that the components of the DIC pool that participate in calcification must not reequilibrate with water immediately before (or during) calcification. The isotopic data imply that the inorganic solids are preserving the solution $HCO_3^-/CO_3^=$ ratio in the $CaCO_3$. One possible explanation is that HCO_3^- can bind to the existing solid and then deprotonate. For the deep-sea corals it is easier to understand why they follow the Usdowski equation. Corals need only precipitate all of the DIC that is present at any time without water reequilibration. This is what McCrea did in his $CaCO_3$ experiment at constant temperature. Vacuole formation and membrane mediation both promote this condition in the coral's mother liquor.

With these two different types of isotopic fractionation for carbon and oxygen, which are both dependent on the pH gradient across the calcifying membrane, the model can explain all parts of the $\delta^{18}O$ vs. $\delta^{13}C$ curves in Figures 2 and 5. Figure
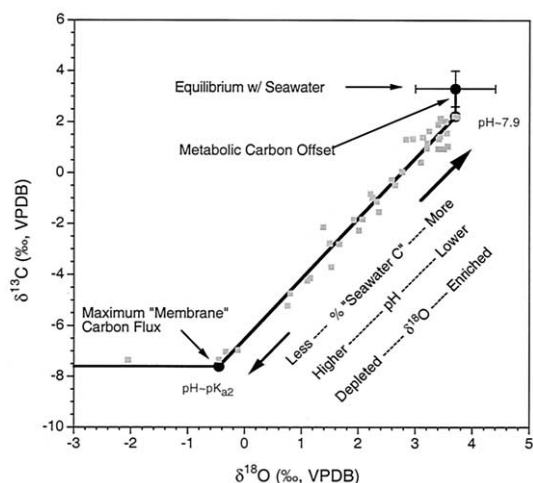
Fig. 9. Schematic representation of the various processes that contribute to the isotopic offsets from equilibrium in deep-sea corals. The skeleton is slightly depleted in $\delta^{13}C$ at $\delta^{18}O$ equilibrium because of a small amount of respired CO_2 in the skeleton. The linear trend between the isotopes results from a mixing of two sources of carbon to the ECF; $CO_{2(aq)}$ that diffuses across the cell membrane and seawater DIC that diffuses in from the surroundings. The same pH gradient that drives membrane diffusion of $CO_{2(aq)}$ also sets the $\delta^{18}O$ value of the precipitating aragonite. Once all of the carbon in the ECF comes from "membrane $CO_{2(aq)}$," the $\delta^{13}C$ cannot get lighter.

9 outlines the skeletal response for a thermodynamic vital effect. Starting at the predicted values for $\delta^{18}O$ and $\delta^{13}C$ equilibrium, there is a small offset in the $\delta^{13}C$ of the skeleton due to metabolic CO_2, from coral respiration, that ends up in the ECF. The large linear trend in $\delta^{13}C$ and $\delta^{18}O$ is created by the balance between two sources of carbon and the different pHs. At the heavy end, the inorganic carbon species of the ECF are dominated by "normally fractionated" seawater and relatively enriched $\delta^{18}O$, a result of the lower pH. At high calcification rates, the DIC of the ECF is dominated by isotopically light carbon from CO_2 that passively diffuses across the calcification membrane because of the large pH and pCO_2 gradients induced by the Ca-ATPase alkalinity pump. Because the proportion of isotopically depleted oxygen from carbonate ion in solution increases relative to bicarbonate ion, this elevated pH also drives the $\delta^{18}O$ of the skeleton lighter. Once the CO_2 gradient gets large enough that the flux of carbon from the membrane crossing CO_2 is at a maximum, the skeletal $\delta^{13}C$ stabilizes. At this point the ratio in the ECF of carbon from surrounding seawater to carbon from across the ECF membrane is constant. However, the alkalinity pump can still drive the pH of the ECF up and continue to create a more carbonate ion enriched environment with its correspondingly lighter $\delta^{18}O$.

4.5. Numerical Model of Deep-Sea Coral Calcification

In the above discussion, the slope of $\delta^{13}C$ vs. $\delta^{18}O$ in coralline aragonite is a balance between calcification at near seawater pHs and calcification at more basic conditions. Equilibrium precipitation from seawater, with a small $\delta^{13}C$ decrease from metabolic carbon, is the isotopically heavy point. However, the $\delta^{13}C$ and $\delta^{18}O$ values of the isotopically depleted

point require a model of the calcification process to better understand their origin. A successful model should explain the constancy of the $\delta^{13}C$ vs. $\delta^{18}O$ slope, the value of this slope and the break from this slope at the lightest values.

Following the schematic in Figure 7, we model the ECF as a box with three inputs and three outputs (Fig. 10). Carbon enters the calcifying region from either a seawater leak or from diffusion of CO_2 across the cell membrane. Each of these exchanges is a two-way process with diffusion coefficients of D_{SW} and D_{Cell}, respectively. Both carbon and alkalinity are removed from the ECF by precipitation of aragonite (F_{CaCO_3}). The enzymatic pump of Ca-ATPase is represented by a flux of alkalinity to the ECF. This alkalinity can be Ca^{++} ion with proton pumping, negative proton pumping alone or some mixture of the two, depending on the value of f_{Ca}. Balances of these fluxes into and out of the ECF for the three conservative properties; DIC concentration, alkalinity (Alk) and calcium concentration ([Ca]), are represented by Eqns. 1 to 3 in Figure 10. Eqn. 4 is the carbonate alkalinity balance. We also constructed models with borate, $[H^+]$, and $[OH^-]$ in the alkalinity expression, but these terms are small relative to the concentrations of carbonate and bicarbonate in all cases. In all equations, H_2CO_3, HCO_3^-, and $CO_3^=$ species are represented by their respective mole fractions; x_0, x_1, and x_2. The last Eqn. 5 describes the flux of aragonite precipitation as an area normalized precipitation that is proportional to the saturation state of the ECF (Inskeep and Bloom, 1985).

Values for the various constants used in the model are listed in Table 3. We solved the model by assuming steady state for a range of enzyme driven alkalinity fluxes ($FAlk_{Pump}$). Given a known pH value, the first four equations of Figure 10 are a system with four unknowns; DIC, Alk, $[Ca^{++}]$, and F_{CaCO_3}. Each steady-state condition was solved by iterating on the pH of the ECF to balance the implied solution for F_{CaCO_3} in Eqns. 1 to 4 with the rate expression of Eqn. 5. Once the pH is known, it is straightforward to calculate the values of the inorganic carbon species. The behavior of the model for three different values of D_{SW}, spanning an order of magnitude in flux, is shown in Figure 11. The ECF starts at near seawater pH and gradually rises as the alkalinity pump is increased. This pH rise drives the $[CO_2]$ in the ECF down, thus increasing the net flux of carbon across the cell membrane ($D_{Cell}[CO_2]_{Cell}-D_{Cell}[CO_2]_{ECF}$). Carbon fluxes from across the cell membrane will increase until the ECF pH is high enough to keep the $[CO_2]_{ECF}$ at such low values that small changes do not effect the net flux. At this point the ratio of carbon from seawater to carbon from the cell within the ECF will be constant. At low values of D_{SW}, the ECF does not have enough ambient seawater to buffer the alkalinity input beyond this point and the pH rises dramatically (Fig. 11). With larger leaks of seawater into the calcifying region, the increase in pH is not as dramatic for a given increase in the alkalinity pump.

Once we have a model of the major inorganic carbon species, it is possible to constrain the ^{13}C mass balance of the ECF. The key equations for this calculation are shown in Figure 10. Here, Rs represent the $^{13}C/^{12}C$ ratio of the various pools and αs represent the standard fractionation factors. ^{13}C input to the ECF is the combination of relatively heavy seawater DIC entering the region ($D_{Sw}DIC_{Sw}R_{Sw}$) and relatively light CO_2 from the cell diffusing across the cell membrane
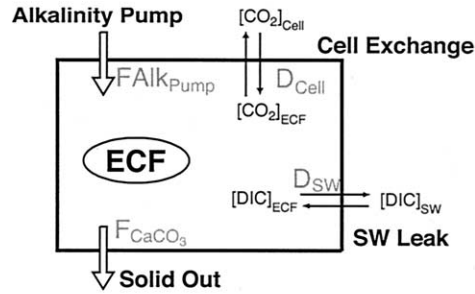
ECF pH Calculation

(1) $$z\frac{\partial DIC_{ECF}}{\partial t} = D_{SW}DIC_{SW} + D_{Cell}[CO_2]_{Cell} - D_{SW}DIC_{ECF} - D_{Cell}DIC_{ECF}x_0 - F_{CaCO_3}$$

(2) $$z\frac{\partial Alk_{ECF}}{\partial t} = D_{SW}Alk_{SW} + FAlk_{Pump} - D_{SW}Alk_{ECF} - 2F_{CaCO_3}$$

(3) $$z\frac{\partial [Ca]_{ECF}}{\partial t} = D_{SW}[Ca]_{SW} + \frac{f_{Ca}FAlk_{Pump}}{2} - D_{SW}[Ca]_{ECF} - F_{CaCO_3}$$

(4) $$Alk_{ECF} = 2DIC_{ECF}x_2 + DIC_{ECF}x_1$$

(5) $$F_{CaCO_3} = \frac{k_{rate}}{Surf}([Ca]DIC_{ECF}x_2 - K_{sp})$$

Carbon Isotope Calculation

$$D_{SW}DIC_{SW}R_{SW} + D_{Cell}[CO_2]_{Cell}R_{CO_2 Cell}\alpha_{Diff} = D_{SW}DIC_{ECF}R_{ECF} + D_{Cell}DIC_{ECF}x_0R_{ECF}\alpha_{Diff}\alpha_{DIC-CO_2} - F_{CaCO_3}R_{ECF}\alpha_{CaCO_3}$$

$$\alpha_{DIC-CO_2} = \frac{\alpha_{CO_2}}{\alpha_{HCO_3-DIC}}$$

$$\alpha_{HCO_3-DIC} = x_0\alpha_{CO_2} + x_1 + x_2\alpha_{CO_3}$$

$$\alpha_{CaCO_3} = \frac{\alpha_{HCO_3-aragonite}}{\alpha_{HCO_3-DIC}}$$

Fig. 10. ECF calcification model schematic and equations. Flux balances for DIC, alkalinity, and [Ca] in the ECF make up Eqns. 1, 2, and 3. Eqn. 4 is the carbonate alkalinity constraint for the ECF. Eqn. 5 is the area normalized rate expression for aragonite precipitation. The fraction of the alkalinity pump that is due to calcium ions (f_{Ca}) allows for both Ca-ATPase and proton ATPase pumps. Symbols used are explained in the text.

($D_{Cell}[CO_2]_{Cell}R_{CO_2}Cell\alpha_{Diff}$). Back flux along both these pathways and precipitation of aragonite ($D_{CaCO_3}R_{ECF}\alpha_{CaCO_3}$) remove ^{13}C. Fractionation factors of the inorganic carbon species were calculated at 5.5°C when the data from Zhang et al. (1995) are used. The fractionation of HCO_3^- relative to DIC is used as a reference point for the other fractionation factors. This value is the weighted mean (using ionization fractions) of the fractionation factors relative to HCO_3^- (Fig. 10). By use of this value (α_{HCO_3}-DIC), the fractionations of CO_2 and aragonite relative to DIC are calculated in the usual manner after using the data of Zhang et al. (1995) to calculate alpha values for CO_2 and $CO_3^=$ relative to HCO_3^-. We use the aragonite to HCO_3^- fractionation of Romanek et al. (1992). The pH dependent oxygen isotope values of the aragonite are calculated according to the equations of Usdowski and Hoefs (1993) as discussed by Zeebe (1999) and then converted to the VPDB scale. The fractionation factors are listed in Figure 8.

Results from these isotopic calculations are shown in Figure 12. For a factor of 10 range in D_{SW}, there remains a constant slope of $\delta^{13}C$ vs. $\delta^{18}O$. The seawater flux is chosen as the parameter to vary because we have a reasonable idea of the cell

permeability to CO_2 (Sultemeyer and Rinast, 1996). However, what really matters is the ratio of $D_{SW}:D_{Cell}$. For small D_{SW} values (black lines in Fig. 12), there are extreme depletions in $\delta^{13}C$. These offsets arise because there is relatively little seawater leaking into the ECF when the pH rises to the point such the $[CO_2]_{ECF}$ is small relative to $[CO_2]_{Cell}$. At this point, the flux of membrane CO_2 is a maximum and is relatively constant. Given a constant seawater leak, the relative ratio of ^{13}C-depleted carbon moving across the membrane to ^{13}C-enriched carbon from seawater is therefore fixed. For small D_{SW} water values, almost the full $\delta^{13}C$ value of CO_2 from the cell is expressed in the solid (and the ECF). For larger values of D_{SW} (dashed and gray lines in Fig. 12), enough seawater is present in the calcifying fluid to dampen the effect of very light cellular CO_2 on the bulk $\delta^{13}C$. However, the pH of the solution can continue to increase and drive down the overall $^{18}O/^{16}O$ ratio on the inorganic carbon species as discussed above. The reason the slope is so constant is shown in Figure 12b. The key control on the $\delta^{18}O$ of the aragonite is the relative abundance of CO_3 in solution relative to HCO_3. The %CO_3, or x_2, is an excellent measure of this parameter at high pH (where $[H_2CO_3]$ is very

Table 3. Values of constants and isotope fractionation factors used in the ECF model.[a]

Variable	Value
Seawater Values	
Alkalinity	2200 μmol/kg
Total carbon	2000 μmol/kg
Flux	Variable
[Ca^{++}]	10300 μmol/kg
Enzyme pump values	
Alk pump	Variable
Ca fraction	1
Cell values	
D_{Cell}	0.0015 cm/s
[CO_2]$_{Cell}$	13 μmol/kg
Carbon system constants	
K_{a1}	8.928×10^{-7}
K_{a2}	5.274×10^{-10}
K_w	8.980×10^{-15}
K_{sp}	6.756×10^{-7}
K_{rate}	118.3
Fractionation factors	
α_{Diff}	1.0007
α_{CO_2}	0.98871
α_{CO_3}	0.99693
$\alpha_{HCO_{3\text{-}arag}}$	1.0027

[a] Seawater values are typical numbers. The diffusion CO_2 across a cell membrane (D_{cell}) is taken from Sultemeyer and Rinast (1996). Carbon system acidity constants are from UNESCO (1987). The precipitation rate constant is from Inskeep and Bloom (1985). Alphas are defined in Figure 10.

low) and is essentially determined by the value of pK_{a2}. The key control on the $\delta^{13}C$ value is the [CO_2] in the ECF, as this is the most important driver of depleted cellular CO_2 into the ECF. Once this value is low enough so that the net flux of CO_2 into the calcifying region is roughly constant, the balance between seawater carbon and cellular carbon is fixed. CO_2 mol fractions are in turn essentially controlled by the value of pK_{a1}. Figure 12 demonstrates that the slope of these two key variables is roughly constant over a large range. The pH where $\delta^{13}C$ stops getting lower is very close to pK_{a2} and the linear trends in Figure 12a arise from the fact that pK_{a1} and pK_{a2} are constant.

Fig. 12. (a) Isotopic values of the aragonite solid for the scenarios in Figure 11. All three model results show a constant slope of $\delta^{13}C$ vs. $\delta^{18}O$ and a break in that slope at the lightest values. (b) Isotopic forcing of oxygen vs. carbon in the ECF. The two important inorganic carbon species in the ECF for calculating the equilibrium $\delta^{18}O$ and $\delta^{13}C$ of aragonite are plotted against each other. For a factor of 10 range in F_{SW}, there is always a large linear region with a relatively sharp break to low [CO_2] at pK_{a2}. See text for discussion.

It is important to point out that Figure 12 only satisfies two of the three criteria outlined above for a successful model. Although we do find a constant slope with a break at the lightest values, we do not calculate the same isotopic slope as observed in the deep-sea corals. This difference is most likely due to the unknown relation between temperature and pH as they influence the $\delta^{18}O$ of $CaCO_3$. Inorganic experiments for both calcite and aragonite that keep track of these two key parameters have only been reliably performed at 19°C (Kim and O'Neil, 1997). Natural variability in the slopes of $\delta^{13}C$ vs. $\delta^{18}O$ can be due to ECFs of differing shape and size. In this case there will be slight variations in the D_{SW}:D_{Cell} ratio, as shown in Figure 12. In addition, some organisms show much smaller ranges of isotopic offset from equilibrium than found in
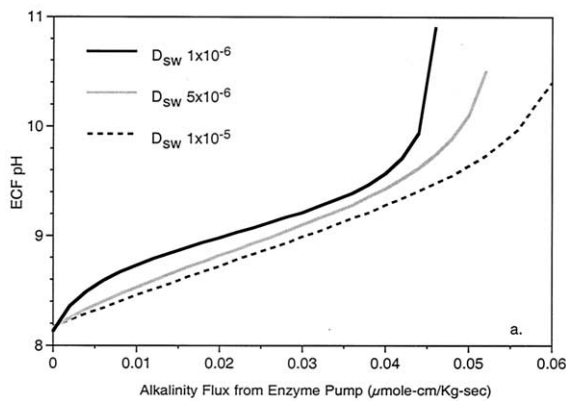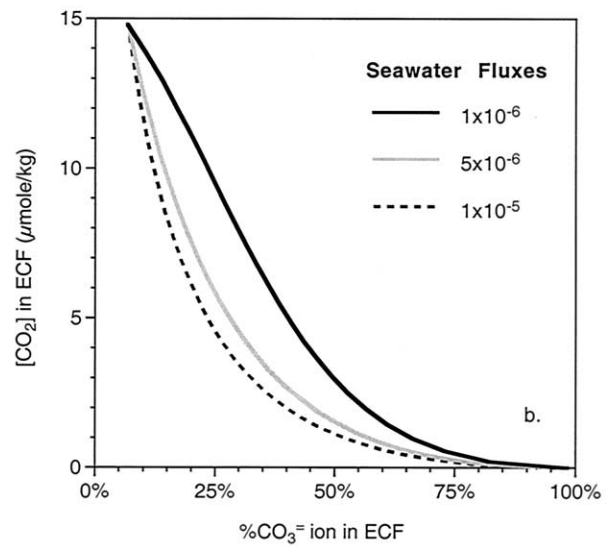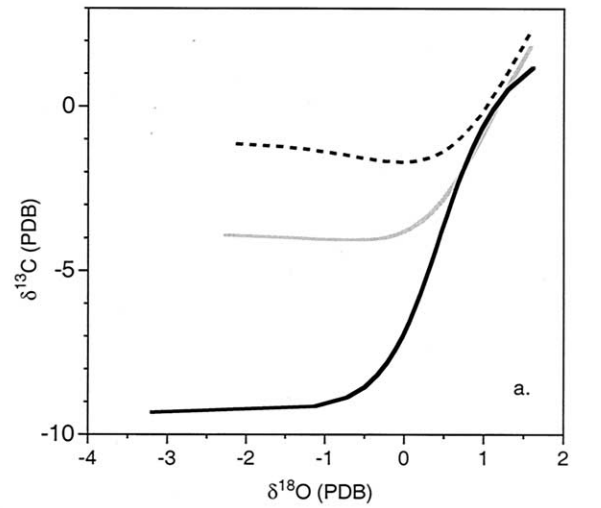

Fig. 11. pH of the ECF as the enzymatic alkalinity pump is increased for three different values of the seawater diffusion coefficient (D_{SW}). In each case, there is a large region of alkalinity flux with constant slope.

these deep-sea corals. Although the slope of $\delta^{18}O$ vs. $\delta^{13}C$ is similar, the calcium carbonate does not move very far down the line. This feature could be due to calcifying environments that are much more influenced by seawater than the deep-sea corals. Foraminifera, for example, make their skeleton in an environment where seawater can easily diffuse into the ECF, but corals have a much more restricted pathway for seawater movement into the calcifying region.

It is often claimed in the literature that calcification rate is the master variable in vital effect offsets. With our mechanism, this is only partially true. pH is the master variable. Higher calcification rates, and a larger vital effect, are correlated with the increase in the coral's alkalinity pump. However, the key to the isotopic fractionation is not the rate of carbonate production but the pH gradient across the calcifying membrane. Once the biology sets the alkalinity input and the geometry of the ECF, the isotopes respond in a thermodynamically predictable way in all carbonates. The fundamental observation for this mechanism is the break in slope seen in Figure 5. Deep-sea corals are unique in their ability to record this process unambiguously because they do not have photosynthetic symbionts, and because they have an ECF that is restricted from large amounts of seawater diffusion. If our model is correct, in any calcification system where there is a pH gradient and an impermeable cell membrane, this isotopic vital effect will be expressed.

5. CONCLUSIONS

Deep-sea corals are unique in their ability to record information about the effects of calcification on $\delta^{18}O$ and $\delta^{13}C$ values. Because of their homogeneous growth environment, lack of photosynthetic symbionts, and large variations in calcification rate, these animals are an unparalleled laboratory for the study of vital effects. At the extreme limit of calcification in the trabecular centers, the ubiquitous linear trend between $\delta^{18}O$ and $\delta^{13}C$ is broken. Because the skeletal morphology implies that this aragonite is formed from the same process as the rest of the coral, a kinetic fractionation mechanism for the isotopic offsets is invalid. Thermodynamic arguments, based on mixing between two separate carbon reservoirs, can explain the data. Enzymatic activity establishes a pH gradient between the impermeable cell wall and the calcifying fluid. This gradient drives a passive CO_2 flux into the ECF and controls the mixing of this carbon with isotopically heavier seawater DIC. Oxygen isotopes also respond to the pH of the ECF. Taken together, this mechanism predicts that any biogenic carbonate formed from a fluid with a pH gradient and an impermeable membrane will show the same effects to a larger or smaller degree.

Associate editor: D. Lea

REFERENCES

Adkins J. F. (1998) *Deep-Sea Corals: A New Ocean Archive.* MIT/ WHOI.

Böhm F., Joachimski M. M., Dullo W. C., Eisenhauer A., Lehnert H., Reitner J., and Worheide G. (2000) Oxygen isotope fractionation in marine aragonite of coralline sponges. *Geochim. Cosmochim. Acta* **64,** 1695–1703.

Broecker W. S. (1986) Oxygen isotope constraints on surface ocean temperature. *Quat. Res.* **26,** 121–134.

Cole J. E., Fairbanks R. G., and Shen G. T. (1993) Recent variability in the Southern Oscillation: Isotopic records from a Tarawa Atoll coral. *Science* **260,** 1790–1793.

Craig H. (1957) Isotopic standards for carbon and oxygen and correction factors for mass-spectrometric analysis of carbon dioxide. *Geochim. Cosmochim. Acta* **12,** 133–149.

Dansgaard W. and Tauber H. (1969) Glacier oxygen-18 content and Pleistocene ocean temperatures 1. *Science* **166,** 499–502.

Druffel E. R. M., Bauer J. E., Williams P. M., Griffin S., and Wolgast D. (1996) Seasonal variabiltiy of particulate organic radiocarbon in the northeast Pacific Ocean. *J. Geophys. Res.* **101,** 20543–20,552.

Duplessy J. C., Lalou C., and Vinot A. C. (1970) Differential isotopic fractionation in benthic foraminifera and paleotemperatures re-assessed. *Science* **168,** 250–251.

Duplessy J.-C., Shackleton N. J., Matthews R. K., Prell W., Ruddiman W. F., Caralp M., and Hendy C. H. (1984) ^{13}C record of benthic foraminifera in the last interglacial ocean: Implications for the carbon cycle and the global deep water circulation. *Quat. Res.* **21,** 225–243.

Emiliani C. (1966) Paleotemperature analysis of Caribbean cores P 6304-8 and P 6304-9 and a generalised temperature curve for the last 425,000 years. *J. Geol.* **74,** 109–126.

Epstein S., Buchsbaum R., Lowenstam H. A., and Urey H. C. (1953) Revised carbonate–water isotopic temperature scale. *Geol. Soc. Am. Bull.* **64,** 1315–1326.

Erez J. (1978) Vital effect on stable-isotope composition seen in foraminifera and coral skeletons. *Nature* **273,** 199–202.

Fairbanks R. G. and Dodge R. E. (1979) Annual periodicity of the $^{18}O/^{16}O$ and $^{13}C/^{12}C$ ratios in the coral *Montastrea annularis. Geochim. Cosmochim. Acta* **43,** 1009–1020.

Furla P., Galgani I., Durand I., and Allemand D. (2000) Sources and mechanisms of inorganic carbon transport for coral calcification and photosynthesis. *J. Exp. Biol.* **203,** 3445–3457.

Gonfiantini R., Stichler W., and Rozanski K. (1993) Standards and intercomparison materials distributed by the International Atomic Energy Agency for stable isotope measurements. Reference and intercomparison materials for stable isotopes of light elements. Proceedings of a consultants meeting held in Vienna, 1–3 December 1993, pp. 13–30.

Goreau T. F. (1959) The physiology of skeleton formation in corals. I. A method for measuring the rate of calcium deposition by corals under different conditions. *Biol. Bull.* **116,** 59–75.

Grossman E. L. and Ku T.-L. (1986) Oxygen and carbon isotope fractionation in biogenic aragonite: Temperature effects. *Chem. Geol.* **59,** 59–74.

Hays J. D., Imbrie J., and Shackleton N. J. (1976) Variations in the Earth's orbit: Pacemaker of the ice ages. *Science* **194,** 1121–1132.

Heikoop J. M., Dunn J. J., Risk M. J., Schwarcz H. P., McConnaughey T. A., and Sandman I. M. (2000) Separation of kinetic and metabolic isotope effects in carbon-13 records preserved in reef coral skeletons. *Geochim. Cosmochim. Acta* **64,** 975–987.

Inskeep W. P. and Bloom P. R. (1985) An evaluation of rate equations for calcite precipitation kinetics at pCO_2 less than 0.01 atm and pH greater than 8. *Geochim. Cosmochim. Acta* **49,** 2165–2180.

Ip Y. K., Lim A. L. L., and Lim R. W. L. (1991) Some properties of calcium-activated adenosine triphosphatase from the hermatypic coral *Galaxea fascicularis. Mar. Biol.* **111,** 191–197.

Johnson K. S. (1982) Carbon dioxide hydration and dehydration kinetics in seawater. *Limnol. Oceanogr.* **27,** 849–855.

Johnston I. S. (1980) The ultrastructure of skeletogenesis in hermatypic corals. *Int. Rev. Cytol.* **67,** 171–214.

Kim S.-T. and O'Neil J. R. (1997) Temperature dependence of $\delta^{18}O$. *Geochim. Cosmochim. Acta* **61,** 3461–3475.

Knutson S. W., Buddemeier R. W., and Smith S. (1972) Coral chronometers: Seasonal growth bands in reef corals. *Science* **177,** 270–272.

Lazier A. V., Smith J. E., Risk M. J., and Schwarcz H. P. (1999) The skeletal structure of Desmophyllum cristagalli: The use of deep-water corals in sclerochronology. *Lethaia* **32,** 119–130.

McConnaughey T. (1989a) ^{13}C and ^{18}O isotopic disequilibrium in biological carbonates: I. Patterns. *Geochim. Cosmochim. Acta* **53,** 151–162.

McConnaughey T. (1989b) ^{13}C and ^{18}O isotopic disequilibrium in biological carbonates: II. In vitro simulation of kinetic isotope effects. *Geochim. Cosmochim. Acta* **53,** 163–171.

McCrea J. M. (1950) On the isotopic chemistry of carbonates and a paleotemperature scale. *J. Chem. Phys.* **18,** 849–857.

McCulloch M., Mortimer G., Esat T., Xianhua L., Pillans B., and Chappell J. (1996) High resolution windows into early Holocene climate: Sr/Ca coral records from the Huon Peninsula. *Earth Planet. Sci. Lett.* **138,** 169–178.

Mook W. G., Bommerson J. C., and Staverman W. H. (1974) Carbon isotope fractionations between dissolved bicarbonate and gaseous carbon dioxide. *Earth Planet. Sci. Lett.* **22,** 169–176.

Ostermann D. R. and Curry W. B. (2000) Calibration of stable isotopic data: An enriched $\delta^{18}O$ standard used for source gas mixing detection and correction. *Paleoceanography* **15,** 353–360.

Ostlund H. G., Craig H., Broecker W. S., and Spencer D. W. (1987) *GEOSECS Atlantic, Pacific, and Indian Ocean Expeditions,* Vol. 7, *Shorebased Data and Graphics.* National Science Foundation.

Pearse V. B. (1970) Incorporation of metabolic CO_2 into coral skeleton. *Nature* **228,** 383.

Romanek C., Grossman E. L., and Morse J. W. (1992) Carbon isotopic fractionation in synthetic aragonite and calcite: Effects of temperature and precipitation rate. *Geochim. Cosmochim. Acta* **56,** 419–430.

Shackleton N. J. (1967) Oxygen isotope analyses and Pleistocene temperatures re-assessed. *Nature* **215,** 15–17.

Smith J. E., Schwarcz H. P., Risk M. J., McConnaughey T. A., and Keller N. (2000) Paleotemperatures from deep-sea corals: Overcoming "vital effects." *Palios* **15,** 25–32.

Sorauf J. E. and Jell J. S. (1977) Structure and incremental growth in the ahermatyic coral *Desmophyllum cristagalli* from the North Atlantic. *Paleontology* **20,** 1–19.

Spero H. J., Bijma J., Lea D. W., and Bemis B. E. (1997) Effect of seawater carbonate concentration on foraminiferal carbon and oxygen isotopes. *Nature* 497–500.

Sultemeyer D. and Rinast K.-A. (1996) The CO_2 permeability of the plasma membrane of *Chlamydomonas reinhardtii:* Mass-spectrometric ^{18}O-exchange measurements form $^{13}C^{18}O_2$ in suspensions of carbonic anhydrase-loaded plasma-membrane vesicles. *Planta* **200,** 358–368.

UNESCO (1987) Thermodynamics of the carbon dioxide system in seawater. *UNESCO Tech. Papers Mar. Sci.* **51,** 1–55.

Urey H. C. (1947) The thermodynamic properties of isotopic substances. *J. Chem Soc.* 562–581.

Usdowski E., Michaelis J., Bottcher M. E., and Hoefs J. (1991) Factors for the oxygen isotope equilibrium fractionation between aqueous and gaseous CO_2, carbonic acid, bicarbonate, carbonate, and water (19°C). *Z. Physik.* **170,** 237–249.

Usdowski E. and Hoefs J. (1993) Oxygen isotope exchange between carbonic acid, bicarbonate, and water: A re-examination of the data of McCrea (1950) and an expression for the overall partitioning of oxygen isotopes between the carbonate species and water. *Geochim. Cosmochim. Acta* **57,** 3815–3818.

Weber J. N. and Woodhead P. M. J. (1972) Temperature dependance of oxygen-18 concentration in reef coral carbonates. *J. Geophys. Res.* **77,** 463–473.

Weidman C. R., Jones G. A., and Lohmann K. C. (1994) The long-lived mollusc *Arctica islandica:* A new paleoceanographic tool for the reconstruction of bottom temperatures for the continental shelves of the northern North Atlantic Ocean. *J. Geophys. Res.* **99,** 18305–18311.

Zeebe R. (1999) An explanation of the effect of seawater carbonate concentration on foraminiferal oxygen isotopes. *Geochim. Cosmochim. Acta* **63,** 2001–2007.

Zeebe R. E. and Sanyal A. (2002) Comparison of two potential strategies of planktonic foraminifera for house building: Mg^{2+} or H^+ removal? *Geochim. Cosmochim. Acta* **66,** 1159–1170.

Zhang J., Quay P. D., and Wilbur D. O. (1995) Carbon isotope fractionation during gas–water exchange and dissolution of CO_2. *Geochim. Cosmochim. Acta* **59,** 107–114.